SIERRA ROTORS: A COMPARATIVE STUDY OF TWO ROTOR EVENTS

Brian J. Billings* and Vanda Grubišić
Desert Research Institute, Reno, NV

1. INTRODUCTION

The Sierra Rotors project (SRP) is the first exploratory phase of a coordinated effort to study mountain waves, rotors, and the attendant phenomena in complex terrain (Grubišić et al. 2004). More information on SRP and its instrumentation is given in Grubišić and Billings (2005a; companion paper 5M.5). A total of sixteen Intensive Observing Periods (IOPs) were conducted during SRP. While evidence of wave activity was found in over half of the IOPs, obvious rotor activity was observed in two events, IOP 8 on 24-26 March (Grubišić and Billings 2005a) and IOP 14 on 20-21 April 2004. (Potential evidence of rotors was observed during other events, but additional analysis would be required to confirm this.)

Both of these events were highlighted by longitudinally long wave clouds which formed slightly downstream of the Sierra Nevada crest (Fig. 1, top). The cloud in IOP 8 appears optically thicker and lower in elevation than in IOP 14. In both events, observations from Owens Valley showed a line of cumulus underneath the lenticular clouds (Fig. 1, bottom). These positions are consistent with roll clouds that form in the updraft of a rotor circulation, indicating that rotors did form in these two wave events.

2. OBSERVATIONS AND NUMERICAL SIMULATIONS

IOP 8 was a 48 hour event from 18 UTC 24 March to 18 UTC 26 March, with a core 24 hour observing period from 12 UTC 26 March to 12 UTC 26 March. IOP 14 was a 21 hour event from 12 UTC 20 April to 09 UTC 21 April. The SRP observations used in the analysis of these two events consist primarily of surface network observations and upstream rawinsonde soundings. More information on wind profiler observations during IOP 8 is given in Cohn et al. (2005). During IOP 14, all mobile equipment was operated from the same locations as in IOP 8. Additional analysis is provided by high-resolution (333 m) numerical simulations from the Naval Research Laboratory's Coupled Ocean/Atmosphere Mesoscale Prediction System (COAMPS^{TM}). Both simulations used identical configurations with the exception of the simulation period and length (Grubišić and Billings 2005a). More detailed information is given in Grubišić and Billings (2005b).

*Corresponding author address: Brian J. Billings, Division of Atmospheric Sciences, Desert Research Institute, Reno, NV 89512; e-mail: billings@dri.edu

3. IOP OVERVIEWS

3.1 *Synoptic Overview*

Both IOPs occurred in the presence of a cyclone located off the WA-BC coast in nearly the same location. Both cyclones would undergo occlusion, with the point of occlusion passing through the Columbia Basin of Washington. Trailing cold fronts extended south and southwestward through Oregon and northern California into the Pacific Ocean. At 700 hPa, both cyclones were associated with strong flow with a westerly component across the Sierra Nevada and speeds of approximately 15-20 m s^{-1}. Holmboe and Klieforth (1957) identify these synoptic conditions as favorable for strong mountain wave events in Owens Valley.

The Sierra Nevada ridgeline is located at approximately 700 hPa. In IOP 8, the 700 hPa flow during most of the event was from a southwesterly direction. Due to the orientation of Owens Valley, this resulted in an optimal flow component normal to the mountain range and a stronger along-valley pressure gradient. The trailing cold front in this event would eventually pass through Owens Valley at 09 UTC 26 March, near the end of the core IOP.

In IOP 14, the 700 hPa flow was from a northwesterly direction throughout the event. This resulted in more of the decomposed flow being directed along the valley and a stronger cross-valley pressure gradient. At the start of the IOP, the trailing cold front was at its nearest point to the valley and was undergoing frontolysis. In subsequent hours, the front would retrograde into the Pacific and continue to weaken. There was no frontal passage during IOP 14.

3.2 *Temporal Evolution*

During both of these events, strong diurnal components of the flow variability was observed, with the waves, rotors, and downslope flow strength reaching the maximum in the late afternoon hours. To illustrate this, in Figures 2a-b, we show the time series of surface observations from AWS station 4 (located in the north central portion of the mesonet; cf. Fig. 3 in Grubišić and Billings 2005a) for the core IOP 8 period and for IOP 14. Both events began with a light and variable surface flow during the early morning hours. By the mid-morning hours, flow had turned to southerly, which is consistent with a thermally forced, upvalley flow at this station. (Stations further up the slopes recorded an easterly, upslope flow.) At nearly the same time in both of these IOPs (13-14 PST[1]), there was a sharp transition to westerly flow and an increase in wind speed. During the evening, there was

[1]PST = UTC - 8 hours

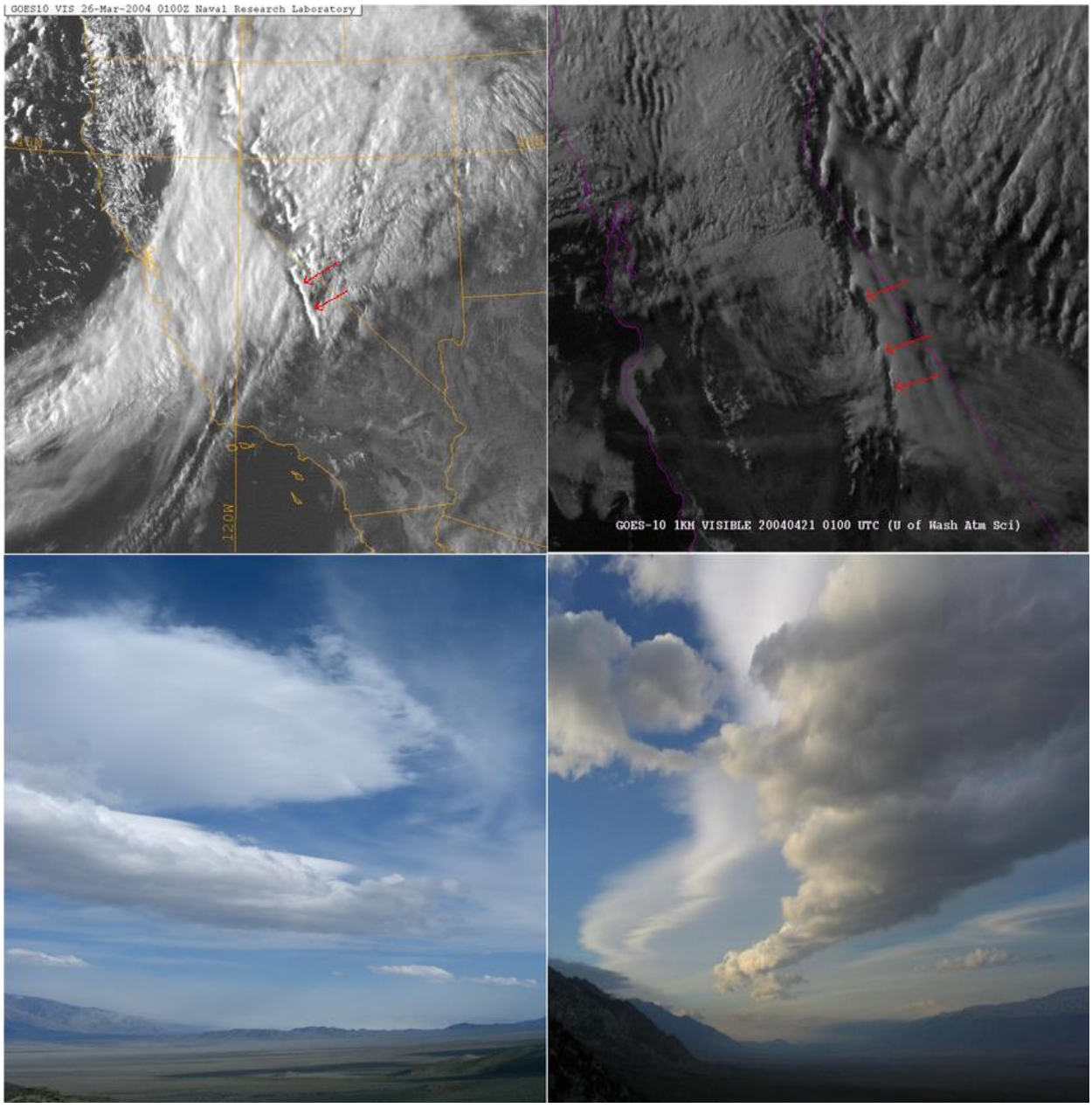

FIG. 1: Top: GOES 10 1 km visible satellite image from (left) IOP 8 at 01 UTC March 26 (17 PST March 25) and (right) IOP 14 at 01 UTC April 21 (18 PST April 20) showing a föhn gap and mountain wave clouds downwind from the Sierra Nevada. Bottom: Photographs from Owens Valley from (left) IOP 8 at 17 PST March 26, looking south from west of Independence (by Vanda Grubišić) and (right) IOP 14 at 19 PST April 20, looking north from west of Lone Pine (by Alex Reinecke).

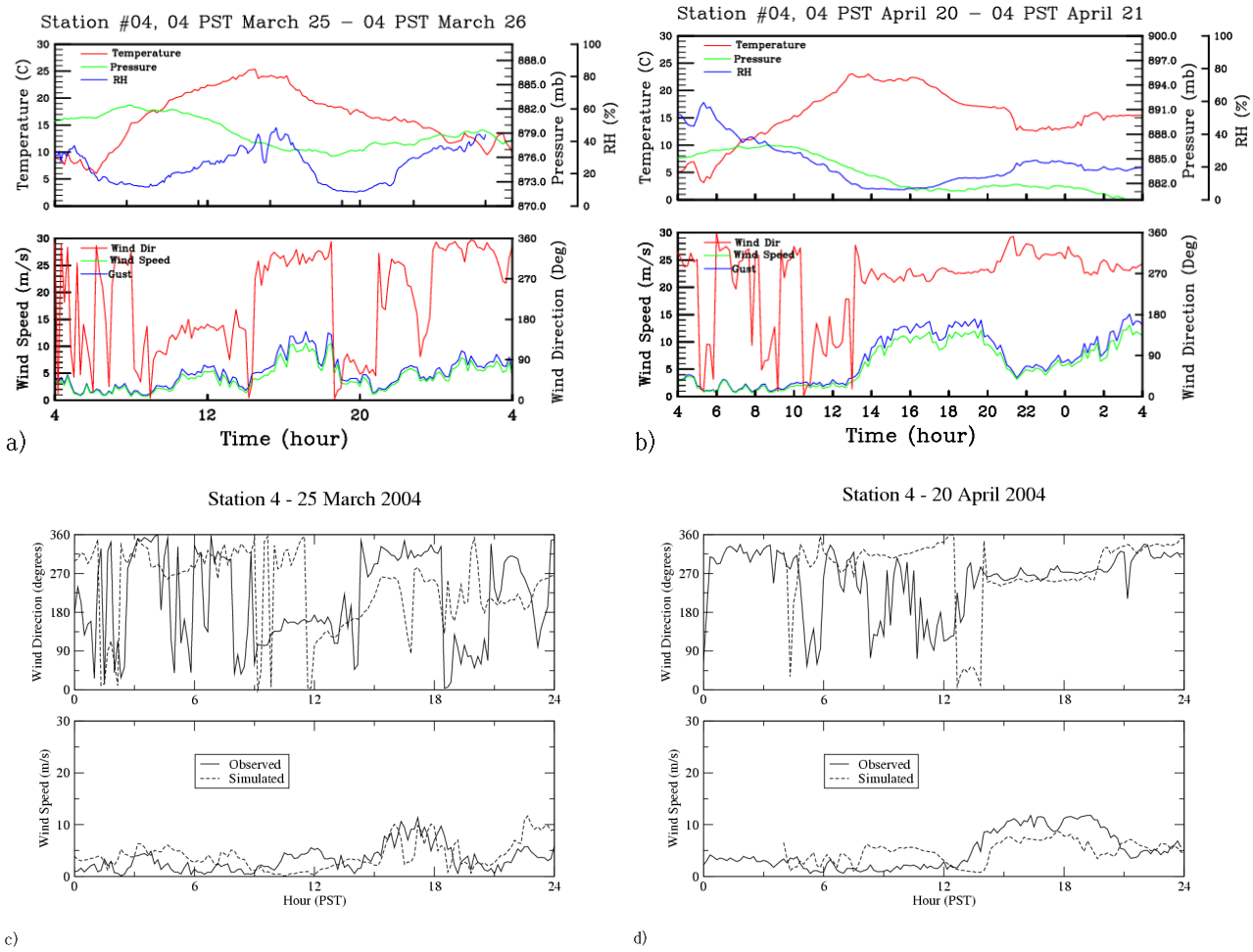

FIG. 2: Time series plots of temperature relative humidity, pressure, and wind speed, gust, and direction measured at station 4 of the ground network during (a) IOP 8 and (b) IOP 14. Time series plots of observed and simulated wind direction and speed during (c) IOP 8 and (d) IOP 14.

a slight decrease in wind speed and an increase in the northerly component of the wind.

While IOP 8 had a better defined thermal circulation period (possibly due to a more favorable synoptic pressure gradient), the primary difference between the two time series occurs at the height of the westerly wind event. During IOP 8, there is a sudden drop in wind speed and shift to easterly flow at station 4, while the wind at stations further up the Sierra Nevada slope remained westerly. Similar change of wind speed and direction at this time was observed at other stations in the central part of the network. This appears to represent the lower half of the rotor circulation extending down to the valley floor. While roll clouds were observed during IOP 14, no reversed flow was observed by the surface network. Therefore, it appears that the rotor remained elevated in this case.

Figures 2c-d compare the observed wind direction and speed with model simualtions. The IOP 8 simulation captures many of the observed features, such as the thermal circulations and sudden shift to westerly flow; however, there is a temporal lag in the simulation. More significantly, the reversed, easterly flow is absent, indicating that the rotor circulation in the model did not extend to the valley floor. The IOP 14 simulation also captures the transition to westerly flow with a slight lag. However, the simulated thermal circulation does not reach this station, and the model overpredicts northerlies at the start of the event. The northerlies near the end of the event do agree well with observations.

4. MOUNTAIN WAVE AND ROTOR ACTIVITY

4.1 *Horizontal Airflow*

As discussed in the previous section, at the height of the mountain wave activity in both events, there was a sharp transition to westerly flow, particularly at the northern line of stations. Figure 3 shows the wind field on the 10 m sigma surface for each event. Both events contain two different types of strong westerly flow. There are strong downslope winds along the eastern Sierra slopes (associated with strong negative vertical velocities there)

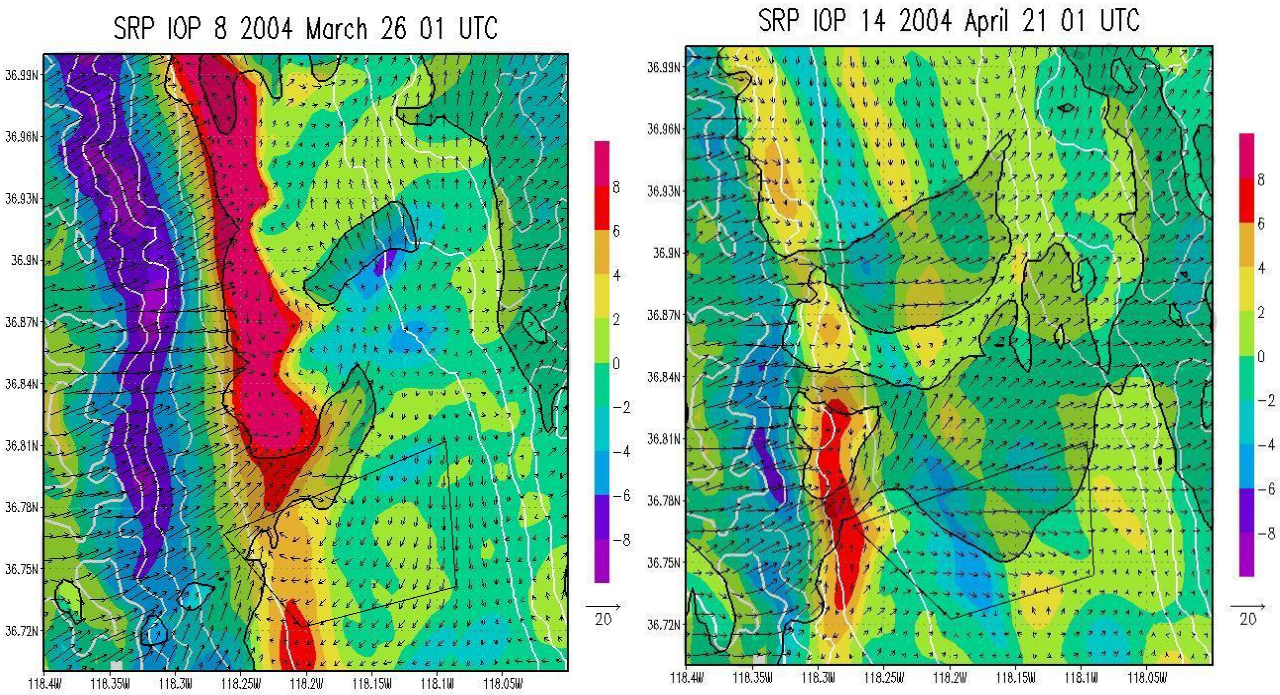

FIG. 3: Terrain (white contours), vertical velocity at 4000 m (color fill), and horizontal wind vectors along the 10 m sigma surface for (a) IOP 8 and (b) IOP 14. The 3500 m contour (thick white) shows the major passes in the Sierra Nevada. Horizontal winds of > 6 m s^{-1} are contoured in black.

that form an unbroken line along the length of the valley, but do not extend much beyond the lower Sierra Nevada slopes. Extending from this line of downslope winds into the valley are gap jets, which can be traced back to major passes in the Sierra Nevada, such as Kearsarge Pass ($\approx$ 36.75° N) and Sawmill Pass ($\approx$ 36.875° N).

In the previous section, it was noted also that a reversed, easterly flow occurred in IOP 8, which was absent in IOP 14. However, there are additional differences in the horizontal flow fields. The observed reduced pressure gradient in IOP 8 is relatively weak, except during the period of reversed flow. In addition, the observed winds at stations further up the Sierra Nevada slopes are as strong as winds observed on the valley floor by station 4, among others. On the other hand, not all of valley floor station reported strong westeries throughout this period. A possible explanation for this surface wind pattern is provided by the numerical simulation. Figure 3 shows that in IOP 8, the downslope winds extended down to the alluvial fan at the western end of the valley, where they were measured by the stations on that lower gradual slope. On the other hand, the gap jet is rather narrow, which means that many stations on the valley floor would not observe the strong westerlies that were observed at station 4.

During IOP 14, the observed reduced pressure gradient was much stronger than in IOP 8, which could be the result of the orientation of the synoptic scale gradient. Furthermore, in this case the winds observed on the valley floor were stronger than the winds observed higher up the slopes, and there were no areas of light winds. Again, the numerical simulations provide a possible explanation. In IOP 14, the strong downslope winds do not extend as far into the valley as in IOP 8 (Fig. 3). However, the two gap jets widen into a broad westerly flow that covers most of the valley floor, but not areas on the slope removed from the passes.

4.2 *Vertical Airflow*

Figure 4 shows a simulated vertical cross-section which transects Owens Valley along the northernmost line of surface stations for the times of observed roll clouds and/or reversed surface flow. Both simulations show a large mountain wave to the lee of the Sierra Nevada with a rotor zone underneath the first wave crest. The areas of rotor activity show a reversed, easterly zonal component and vertical isentropes, indicating a well-mixed region.

The wavelength of the mountain waves observed during IOP 8 was highly variable within the 24 hour core observing period. During the height of the event, the IOP 8 mountain wave featured a long resonant wavelength equal to the width of the valley. The first wave crest is positioned over the center of the valley, which is consistent with the reversed flow being observed at station 4. Also, the wave trough is located far down the Sierra Nevada slopes, where it was observed as an area of low pressure by the mesonetwork and more penetrating downslope winds.

In IOP 14, the wavelength of the mountain wave was far less variable. The wavelength was also much shorter, with the first wave crest covering only half of the valley. The wave crest and rotor zone is located further

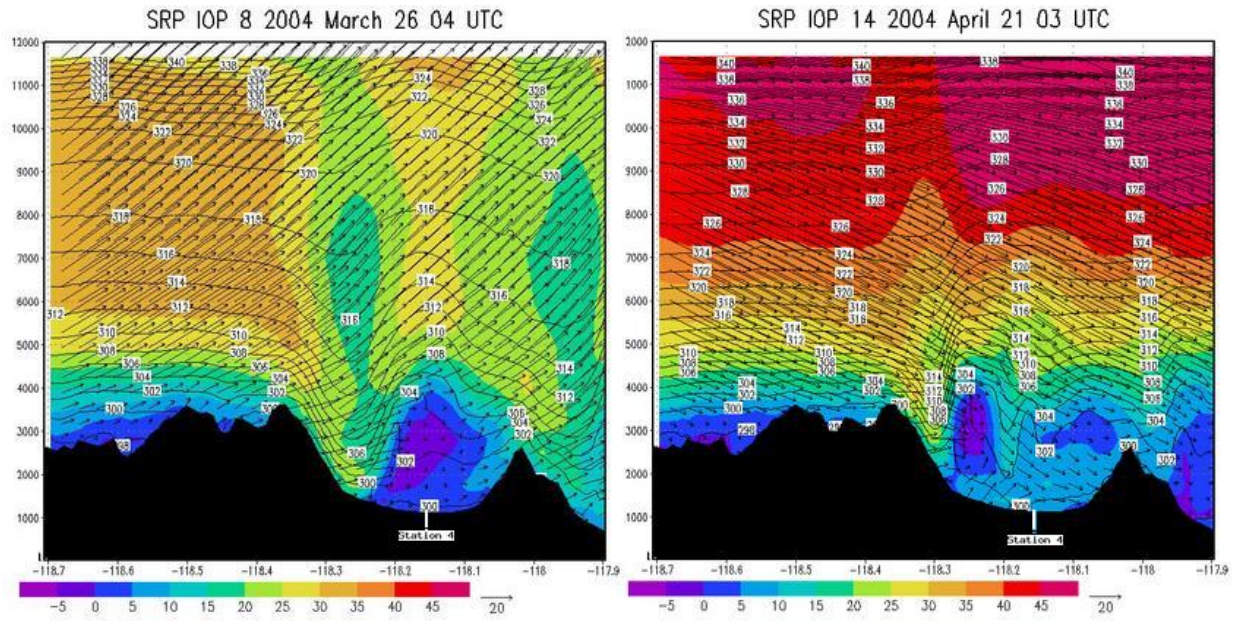

FIG. 4: Vertical cross-section of horizontal wind vectors (m s^{-1}), isentropes (K), and zonal wind speed (m s^{-1} in color) through northern line of stations for (a) IOP 8 and (b) IOP14.

up the slopes, and higher pressures were observed by the mesonet. The wave trough in this case is located far up the Sierra Nevada slopes, and the strong downslope winds associated with it would likely not be observable by the surface stations.

5. WAVE PROPAGATION REGIMES

Figure 4 shows that when rotor activity occurs in Owens Valley, wave activity is trapped at lower levels. Scorer (1949) first showed that this can occur where stability decreases and wind speed increases rapidly with height. Upstream rawinsonde soundings at 12 UTC (not shown) for both cases show this characteristic in a layer near 500 hPa. A sharp increase in wind speed corresponds to an abrupt change in stability, due to a dry-adiabatic layer in IOP 8 and a temperature inversion in IOP 14. Vosper (2004) showed that near-mountain inversions could have a large impact on lee wave activity, but an unstable layer aloft could also result in a large stability decrease.

MGAUS soundings near the end of IOP 14 show the same upstream structure, though the inversion has descended over time. Consequently, wave trapping was observed throughout IOP 14. However, in IOP 8, a frontal passage occurred near the end of the core observing period. This led to a change in the upstream profile, producing the stability and wind speed profiles that were more constant with height. Subsequently, both wind profiler observations (Cohn et al. 2005) and numerical simulations show more vertical wave propagation, and even wave breaking, after the frontal passage had occurred (Fig. 5).

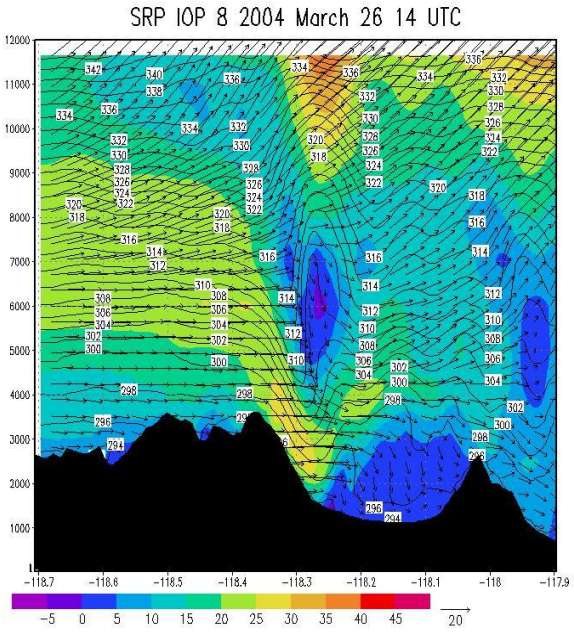

FIG. 5: Vertical cross section of horizontal wind vectors, isentropes, and zonal wind speed through northern line of stations for 14 UTC 26 March 2004.

6. SUMMARY AND IMPLICATIONS

During the Sierra Rotors project, two rotor events were confirmed by visual observations from the ground, in IOP 8 and IOP 14, which were analyzed here. Both events formed in synoptic environments with strong cross-mountain flow and ahead of a cold front. The two events featured the same diurnally varying sequence of wind regimes: from light, variable winds during the early morning through thermally driven flow during the mid-morning and mid-day to strong westerlies in the afternoon. Both events featured a combination of strong downslope winds and gap jets in the surface wind field. Finally, both events began with significant wave trapping, which is the environment in which the rotors are expected to form.

IOP 8 culminated in reversed, easterly flow observed at the surface. The event formed in SW flow and a frontal passage occurred near the end of the core observing period. Observed pressure gradients were weaker, and the surface flow featured more penetrating downslope flow and narrower gap jets. At its peak strength, the mountain wave had a resonant wavelength, and the first of the wave crests was positioned over the valley center. The early wave trapping was aided by an unstable layer aloft ($>$ 500 hPa). The frontal passage unlocked the trapping and the wave activity transitioned into a more vertically propagating event.

IOP 14 did not feature a reversed surface flow. The event formed in NW flow, and the cold front remained offshore. Surface pressure gradients observed by the mesonetwork were stronger in this event, and the surface flow featured less penetrating downslope flow, but broader gap jets. The mountain wave was shorter in wavelength, and the first crest was positioned further up the eastern Sierra Nevada slopes. The wave trapping in this case was aided by a temperature inversion aloft, and the wave trapping remained in place throughout the IOP.

The results of this study have implications for future research, particularly the upcoming Terrain-induced Rotor Experiment (T-REX; Grubišić et al. 2004). First, it appears that the strongest rotor events form under common synoptic conditions (i.e., strong cross-mountain flow, a stable, pre-frontal environment, and often a strong mountain top inversion). Also, most rotor and other wave events involve a strong diurnal component, with a decoupled boundary layer in the morning hours, giving way to strong wave activity in the afternoon. However, different rotor events can have different characteristics, including variable wavelengths, downslope wind penetrations into the valley, and gap jet widths. This spatial variability will require varying observational strategies. The center of the valley was ideal for sampling the rotor zone in IOP 8, but in IOP 14 it would have been beneficial for the instruments, both surface stations and wind profilers, to be further upslope. Mobile equipment is ideal under such circumstances. However, in order to be able to predict the nature of future events, including the wavelength of the mountain wave and location of rotors within the valley, it will be important to identify what factors determine the specific event characteristics.

ACKNOWLEDGMENTS

The high-resolution real-data COAMPS run were carried out on the Mesoscale Dynamics and Modeling Laboratory's 68-processor Sierra cluster at DRI funded by the NSF grant ATM-0116666. This research was supported in part by the NSF grant ATM-0242886. The SRP was a joint effort between DRI, NRL, and the University of Washington. We thank Dale Durran, Jim Doyle, Qingfang Jiang, Steven Cohn, and Bill Brown for their efforts during the SRP field phase and Ming Xiao for the analysis of the surface observations.

REFERENCES

Cohn, S. A., W. O. J. Brown, V. Grubišić, and B. J. Billings, 2005: The signature of waves and rotors in wind profilers: Results of the Sierra Rotors Project. *Online Preprints: 32nd Conference on Radar Meteorology.* Amer. Meteor. Soc., Paper **2R.6.**

Grubišić, V., and B. J. Billings, 2005a: Sierra Rotors: A study of the IOP 8 rotor event. *Online Preprints: 11th Conference on Mesoscale Processes.* Amer. Meteor. Soc., Paper **5M.5**

——, and B. J. Billings, 2005:b A numerical study of the Sierra Rotors IOP 8 event. In preparation.

——, J. D. Doyle, J. Kuettner, G. S. Poulos, and C. D. Whiteman, 2004: Terrain-induced Rotor Experiment. Scientific Overview Document and Experiment Design. 72 pp. Available at http://www.joss.ucar.edu/trex/

Hodur, R. M., 1997: The Naval Research Laboratory's Coupled Ocean/Atmosphere Mesoscale Prediction System (COAMPS). *Mon. Wea. Rev.,* **111,** 1414-1430.

Holmboe, J. R., and H. Klieforth, 1957: Investigation of mountain lee waves and the airflow over the Sierra Nevada. Final Report. Department of Meteorology, UCLA, Contract AF 19(604)-728, 283 pp.

Scorer, R. S., 1949: Theory of lee waves of mountains. *Q. J. R. Meteorol. Soc.,* **75,** 41-56.

Vosper, S. B., 2004: Inversion effects on mountain lee waves. *Q. J. R. Meteorol. Soc.,* **130,** 1723-1748.